Kinetically Driven Growth Instability in Stressed Solids

William Barvosa-Carter* and Michael J. Aziz†
Division of Engineering and Applied Sciences, Harvard University, Cambridge, Massachusetts 02138

L. J. Gray and Theodore Kaplan
Computer Science and Mathematics Division, Oak Ridge National Laboratory, Oak Ridge, Tennessee 37831
(Received 10 April 1998)

We report a new stress-induced kinetically driven morphological instability for driven systems. The effect of stress on the interfacial mobility couples to stress variations along a perturbed planar growth front. Comparison of theory and experiment for solid phase epitaxy at a corrugated Si(001) interface, with no free parameters, indicates that the new mechanism is required to account for the observed growth of the corrugation amplitude. This mechanism operates in conjunction with known diffusional and elastic strain energy-driven instabilities in determining morphological evolution. [S0031-9007(98)06924-5]

PACS numbers: 61.50.Ks, 68.35.Bs, 68.35.Ct, 82.20.Mj

There is increasing interest in the effects of nonhydrostatic stresses on condensed phase processes such as diffusion and crystal growth. The focus of most work has been to understand and account for stress effects on the energetics, or driving forces, for these processes, particularly in recent studies of the morphological stability of stressed solids. The surfaces of stressed solids are generally subject to an elastic strain energy-driven morphological instability [1], the characterization of which has been the focus of much recent effort, especially under conditions of strained heteroepitaxial thin film growth [2]. However, the growth and morphology of a solid is determined not only by the energetics of the relevant phases but also by the mobilities of the interfaces or atoms involved in growth. Little attention has been paid to stress effects on mobilities, largely due to experimental difficulties associated with isolating mobility effects from driving force effects. In particular, the processes by which stress-dependent mobilities might affect growth morphology have been entirely ignored. In this Letter, we report a new morphological instability that is driven by the stress dependence of mobilities during growth.

Within transition state theory, the dependence upon stress, $\boldsymbol{\sigma}$, of an atomic or interfacial mobility, M, is characterized by the *activation strain tensor* $V_{ij}^{*} = kT\partial \ln M/\partial \sigma_{ij}$ [3]. A positive (negative) V_{11}^{*}, for example, implies that M is reduced (enhanced) upon the application of a compressive (tensile) σ_{11}. Just such a dependence of the interface mobility has been observed in solid phase epitaxial growth (SPEG) in Si(001) [4].

We have identified a new, *kinetically driven* morphological instability arising from a growth situation in which the mobility is reduced by stress. With stress relaxation in the amorphous (parent) phase (Fig. 1) and at the apex of a perturbation in a growing crystalline phase, and stress concentration in the trough, the mobility at the apex is greater than at the trough. Hence the apex grows fastest and the perturbation tends to amplify.

The destabilizing effect of a stress-dependent mobility can be of lower order in stress than that of stress-dependent energetics. Typically for small driving force F, the growth rate v is the product of M and F, both of which can be expanded in powers of σ. The destabilizing term from the elastic strain energy-driven instability is of the order of σ^2 in the expansion of F. The destabilizing term from a stress-dependent mobility is of the order of σ^1 in the expansion of M. Moreover, for the kinetically driven instability, if the interface is unstable for a given stress state, then it is necessarily *stable* for the opposite stress state. The energetically driven instability, in contrast, is predicted to occur for stress of either sign.

We examine this new instability experimentally using SPEG of Si(001) as our model system—the only system at present for which $\mathbf{V}^{*}$ has been measured. Also, because nearly all of the other important parameters characterizing SPEG are known, quantitative predictions concerning the evolution of the amorphous-crystal (a-c) interface are possible with no adjustable parameters.

While spontaneous roughening under stress of an initially planar Si(001) a-c interface, which never roughens in the absence of stress, is observable, the results are difficult to quantify under the range readily accessible experimental conditions because of sample breakage. Instead, we applied stress to a "prerippled interface" fabricated by

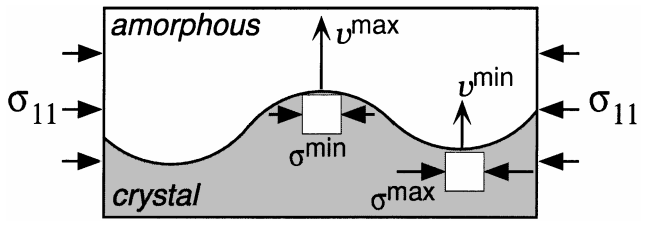

FIG. 1. Origin of instability. If compressive stress reduces interface mobility, then during growth under compression, stress relaxation at peak and stress concentration in valley cause peak to grow faster and perturbation to amplify.

ion implantation of a Si wafer with a lithographically corrugated free surface. By controlling the amplitude and wavelength of the starting interface corrugation, we can make a controlled comparison between theory and experiment for the interface evolution under stress.

Several Si(001) wafers 1 mm thick were patterned using x-ray lithography to create free surfaces corrugated with lines parallel to either [110] or [100] and repeat lengths of $\lambda = 200$ or 400 nm. Each wafer's surface was then amorphized by ion implantation (Si^+, 90 keV, $2 \times 10^{15}/cm^2$, 77 K) to form a continuous layer of amorphous Si (a-Si). Because of straggling of incident ions, the initial 20 and 25 nm surface corrugation amplitudes for the 200 and 400 nm samples, respectively, resulted in 13.5 and 22 nm corrugation amplitudes for the a-c interface. The samples were then diced to form bars 6 mm long with a 1 mm^2 cross section and the a-Si film occupying one of the long faces and the ripples parallel to the short edge. A series of samples was annealed at 520 °C while compressed lengthwise, resulting in a uniaxial stress of -0.5 GPa in the plane of the interface. A control series was annealed under zero stress. The stress-annealing apparatus is described elsewhere [4]. All samples were analyzed using cross-sectional transmission electron microscopy.

In Fig. 2 we show the corrugated interface before and after growth in the presence and absence of stress. The corrugation amplitude increases during growth under stress and decreases during growth under stress-free conditions, in qualitative agreement with both the energetically driven and the kinetically driven mechanisms. The reduction of the corrugation amplitude is expected during growth in the absence of stress because of capillarity and because of growth kinetic anisotropy: orientations away from (001) grow slower; hence the (001) troughs "catch up" while the (001) peaks "grow themselves out of existence."

In Fig. 3 we compile the results for several samples of 400 nm repeat distance. The reported amplitude of the interface corrugation is normalized by the amplitude of the surface corrugation because of sample-to-sample variations in the latter. There is a significant difference between growth under stress and stress-free growth [5].

For a quantitative comparison of theory and experiment, we developed an interface shape evolution algorithm fully capable of handling all the complexities such as growth kinetic anisotropy and the nonlinear velocity-driving force relation at large driving forces. The interface is represented as a series of intersecting line segments [6]. Each segment's velocity normal to itself is determined by the following function of the local conditions (orientation, mean curvature, stress) at its midpoint:

$$v \propto \left[f(\theta) \exp\left(\frac{-G^*}{kT}\right)\right]\left[2 \sinh\left(\frac{-\Delta G_{ac}}{2kT}\right)\right], \quad (1)$$

where $f(\theta)$ is the growth kinetic anisotropy function of misorientation, θ, from (111), G^* is the Gibbs free energy of activation, ΔG_{ac} is the change in free energy per atom crystallized, and κ is the interface curvature. The first bracketed factor in (1) is the mobility and the second is the thermodynamic, or driving force, factor. After each iteration, end points are identified by extrapolating the line segments until they intersect. Segments are deleted if overgrown by neighbors. A segment is split into two if there is a sufficiently large difference in the velocity function of the conditions of its end points.

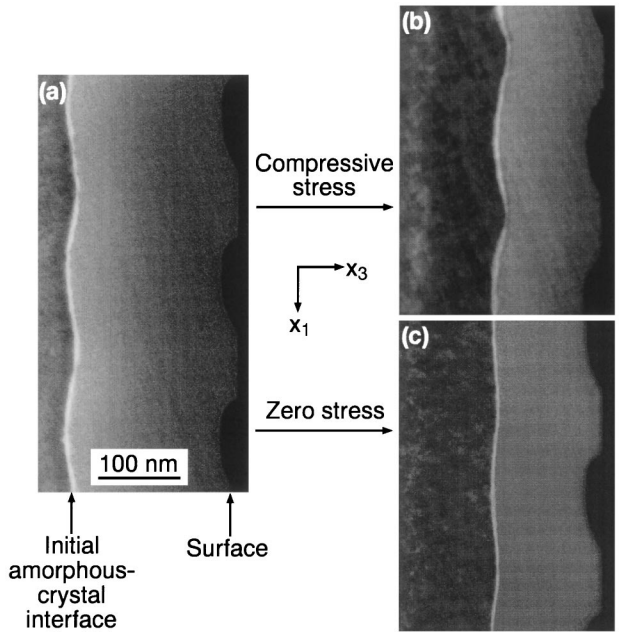

FIG. 2. Cross sections of (a) Initial interface. (b) Interface after 100 nm growth under stress ($\sigma_{11} = -0.5$ GPa) showing amplification of perturbation. (c) Interface after 100 nm growth stress-free showing damping of perturbation.

The local stress state is determined by a boundary integral method [7]. Given a set of tractions and displacements as boundary conditions, and the elastic constants of the solid, the remaining unknown surface displacements and tractions are obtained through solving boundary integral equations. The full stress tensor on the boundary is then computed using the formulation presented in [8].

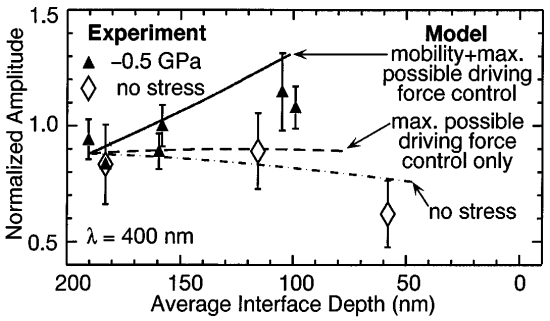

FIG. 3. Perturbation amplitude vs distance grown.

This stress solution is obtained for conditions of plane stress, which is the best approximation to the stress state of the experimental samples.

The ingredients that are input into the evolver are the kinetic coefficients obtained from the literature. The activation strain tensor describes the stress dependence of G^*. Measurements for (001) yield first and second diagonal elements of $+0.14\ \Omega$ and a third diagonal element of $-0.35\ \Omega$, where Ω is the atomic volume of the crystal; off-diagonal elements are zero [4,9,10]. As the interface orientation varies, the atomistic processes occurring at the interface that determine the activation strain tensor are assumed to retain their orientation with respect to the lattice (which would result if, e.g., all action occurred at step edges), resulting in $\mathbf{V}^*$ and G^* fixed to the lattice and independent of interface orientation. The kinetic anisotropy [11] is taken [10] as varying as $\sin|\theta|$ with $v_{001}/v_{111} = 20$. ΔG_{ac} is the sum of several terms,

$$\Delta G_{ac} = \Delta G_{ac}^{o} + \Delta G_{\kappa} + \Delta G_{\sigma}^{(pV)} + \Delta G_{\sigma}^{(ec)} - \Delta G_{\sigma}^{(ea)}.$$

ΔG_{ac}^{o} is the stress-free difference in bulk free energies. ΔG_{κ} is the effect of curvature on driving force, calculated using the "weighted mean curvature" method [6] for each segment along the interface. The interfacial tension is assumed equal to $0.45\ \mathrm{J/m^2}$ and isotropic [12,13]. There are three distinct contributions due to stress. $\Delta G_{\sigma}^{(pV)}$ is the pV work due to the interaction of the hydrostatic component of the stress state with the volume drop upon crystallization of 1.8% [14]. $\Delta G_{\sigma}^{(ec)}$ and $\Delta G_{\sigma}^{(ea)}$ are the increases in elastic energy of the crystal and amorphous phases, respectively, due to stress. The stress is assumed to be fully relaxed in the amorphous phase, i.e., $\Delta G_{\sigma}^{(ea)} = 0$. Incomplete relaxation, which we know to be the case in reality [15], will reduce the amplification rate of a perturbation; hence our calculations provide a theoretical upper limit on the amplification rate [16].

In the absence of stress, growth, or anisotropy, this model correctly reproduces classical relaxation kinetics [17], in which the amplitude decay is exponential in time with a time constant proportional to the square of the wavelength [18]. It also produces the expected behavior for stress-free growth with kinetic anisotropy [10].

For growth in the presence of anisotropy and stress, a sinusoidal perturbation is predicted to decay in the absence of stress and increase in the presence of compressive stress. The predicted shape of the growth front in the presence of stress is sharper at the peaks and flatter in the troughs, as was observed in Fig. 2(b). The rates of growth and decay of the corrugation amplitude for 0.5 GPa are compared to the experimental rates in Fig. 3 (solid curve). Also shown in Fig. 3 are the predictions for driving force control only, which are obtained by setting the activation strain to zero, leaving only the energetically driven instability. Significantly, because both curves are theoretical upper limits due (mainly) to the assumption of complete stress relaxation in the amorphous phase, the data cannot be reconciled with the energetically driven instability alone. We emphasize that the energetically driven instability is suppressed by capillarity and kinetic anisotropy, and that therefore the kinetically driven interfacial instability is required to explain the observed growth of these perturbations [19].

The influence of $G^*(\boldsymbol{\sigma})$ in Eq. (1) is increasingly destabilizing at shorter wavelengths. A fastest growing wavelength may be selected by a variety of other factors. Capillarity may suppress the instability at short wavelengths. For SPEG of (001) Si, however, whether this occurs depends on the functional form of the thermodynamic factor [9,10]. If long-range mass transport (not present for SPEG) contributes to overall rate limitation, its presence in the shrinking phase will reduce the instability growth rate at long wavelengths, and its presence in the growing phase will act as a stabilizing influence [20]. Growth kinetic anisotropy may select an aspect ratio, rather than a wavelength, depending on the functional form of $f(\theta)$ in Eq. (1): Our simulations show short wavelengths growing slower as the aspect ratio increases.

This kinetically driven instability is of general applicability to any kinetically evolving system. Phenomenologically, V_{11}^* will be either positive or negative. Systems with positive (negative) V_{11}^* tend to instability in the presence of negative (positive) σ_{11}, i.e., when the sign of the stress state is such as to lower the interface mobility. The same instability should occur in the presence of surface diffusion such as in molecular beam epitaxy growth. The mechanism described above will operate on the rate constants for the incorporation of mobile species into the crystal (e.g., on the Ehrlich-Schwoebel barriers for attachment at steps), resulting in a dependence of the local growth rate on the local stress state. Additionally, there should be a kinetically driven island shape instability analogous to that presented here for surfaces: a shape fluctuation in a growing or shrinking island should give rise to stress variations along its perimeter, possibly reducing the attachment barrier and thereby increasing the flux at the protuberances. This kinetically driven island instability would be complementary to an energetically driven instability in which elastic strain energy reduction pays for increased island perimeter [21], and a diffusional instability originating from greater diffusional fluxes at the protuberances [22]. In general, this new instability can play a role in 2D island growth or shrinkage or in step-flow terrace growth, if there is an attachment barrier and a stress at the step; this can happen even in homoepitaxial situations due to the self-stress associated with a step.

During "quantum dot" formation a related kinetic mechanism may play a role in limiting the size of a coherently strained island by altering the barrier to atom attachment [23] at the island perimeter. If the attachment barrier is raised by compressive stress, such a mechanism would favor the narrow island size distributions seen during the self assembly of quantum dots [24].

Not only would the energetically and kinetically driven mechanisms produce a different time dependence of the island size, but they would also predict different behavior when the sign of the stress state is reversed.

This sign reversal in the kinetically driven instability when the sign of the stress state reverses, in contrast to that of the energetically driven instability, is a prediction that can be tested for many growth processes without knowledge of all of the parameter values required for a quantitative comparison such as the one presented here for SPEG. Along these lines, the kinetically driven instability mechanism may offer a different interpretation than has been advanced to date [25,26] for the observation that the MBE growth morphology of $Si_{1-x}Ge_x$ on $Si_{0.5}Ge_{0.5}$ is rough for growth under biaxial compression and smooth under tension.

In summary, a new stress-induced growth instability mechanism is of general applicability to driven systems in which the growth front is out of local equilibrium. A quantitative comparison of theory and experiment for Si(001) SPEG with no free parameters indicates that the mechanism is required for an explanation of the observed growth of a perturbation. This mechanism must be considered in conjunction with the energetically driven and diffusional instability mechanisms when predicting morphological evolution in nonequilibrium systems.

We thank W. Craig Carter for helpful discussions in the development of the interface evolution algorithm. We thank H. I. Smith for providing facilities and J. Carter for technical assistance with x-ray lithography at MIT. We acknowledge valuable discussions with J. Tersoff about the role of long-range diffusion. This research was supported initially by NSF-DMR-95-26583 and the Harvard MRSEC, and subsequently by NSF-DMR-95-25907. Work at ORNL was supported by the Applied Mathematical Sciences Research Program, U.S. DOE, under Contract No. DE-AC05-96OR22464 with Lockheed Martin Energy Research Corp.

*Present address: Naval Research Laboratory, Code 6177, Washington, D.C. 20375.

†Email address: maziz@harvard.edu

[1] R. J. Asaro and W. A. Tiller, Metall. Trans. **3**, 789 (1972); M. A. Grinfeld, Sov. Phys. Dokl. **31**, 831 (1986); D. J. Srolovitz, Acta Metall. **37**, 621 (1989).

[2] H. Gao, J. Mech. Phys. Solids **42**, 741 (1994); J. E. Guyer and P. W. Voorhees, Phys. Rev. Lett. **74**, 4031 (1995).

[3] M. J. Aziz, P. C. Sabin, and G.-Q. Lu, Phys. Rev. B **44**, 9812 (1991).

[4] W. B. Carter and M. J. Aziz, Mater. Res. Soc. Symp. Proc. **356**, 87 (1995).

[5] No significant difference was observed between [110] and [100] ripples.

[6] J. E. Taylor, J. W. Cahn, and C. A. Handwerker, Acta Metall. Mater. **40**, 1443 (1992); J. E. Taylor, Acta Metall. Mater. **40**, 1475 (1992).

[7] J. H. Kane, *Boundary Element Analysis in Engineering Continuum Mechanics* (Prentice-Hall, Englewood Cliffs, NJ, 1998).

[8] L. J. Gray, D. Maroudas, and M. N. Enmark, Comp. Mech. (to be published).

[9] W. Barvosa-Carter and M. J. Aziz, Mater. Res. Soc. Symp. Proc. **441**, 75 (1997).

[10] W. Barvosa-Carter, Ph.D. thesis, Harvard University, 1997.

[11] L. Csepregi, E. F. Kennedy, J. W. Mayer, and T. W. Sigmon, J. Appl. Phys. **49**, 3906 (1978).

[12] C. M. Yang, Ph.D. thesis, California Institute of Technology, 1997.

[13] N. Bernstein, M. J. Aziz, and E. Kaxiras, Phys. Rev. B (to be published).

[14] J. S. Custer *et al.*, Appl. Phys. Lett. **64**, 437 (1994).

[15] A. Witvrouw and F. Spaepen, J. Appl. Phys. **74**, 7154 (1993).

[16] The thermodynamic factor involving driving free energy—the sinh factor in Eq. (1)—is also chosen (in favor of its common alternative $[1 - \exp(\Delta G_{ac}/kT)]$) in order to provide a theoretical upper limit on the increase in amplification rate due to changes in ΔG_{ac}.

[17] W. W. Mullins, J. Appl. Phys. **30**, 77 (1959).

[18] When the amorphous phase is completely stress relaxed, SPEG is equivalent to growth from the vapor under "evaporation-condensation" kinetics (Ref. [17]).

[19] Theoretical upper-limit predictions both with and without a nonzero $\mathbf{V}^*$ for samples with 200 nm repeat distance exceeded the observed amplification rate. We attribute this to less complete stress relaxation of the amorphous phase when the corrugation wavelength is shorter.

[20] C. Wagner, J. Electrochem. Soc. **103**, 571 (1956); G. Grinstein, Y. Tu, and J. Tersoff (unpublished).

[21] J. Tersoff and R. M. Tromp, Phys. Rev. Lett. **70**, 2782 (1993).

[22] W. W. Mullins and R. F. Sekerka, J. Appl. Phys. **35**, 444 (1964); G. S. Bales and A. Zangwill, Phys. Rev. B **41**, 5500 (1990).

[23] This atomic migration barrier is to be distinguished from the barrier to "critical nucleus" formation (Ref. [26]).

[24] Y. Chen and J. Washburn, Phys. Rev. Lett. **77**, 4046 (1996); G. Medeiros-Ribeiro *et al.*, Science **279**, 353 (1998); D. E. Jesson, G. Chen, K. M. Chen, and S. J. Pennycook, Phys. Rev. Lett. **80**, 5156 (1998).

[25] Y.-H. Xie *et al.*, Phys. Rev. Lett. **73**, 3006 (1994).

[26] J. Tersoff, Phys. Rev. Lett. **74**, 4962 (1995).